

Composite Materials with Enhanced Conductivities

By Hanxing Zhu,* Tongxiang Fan and Di Zhang

The authors have analyzed the isotropic thermal/electrical conductivities of two types of specially structured composite materials. Closed-form results have been obtained for predicting the conductivities of the composites, and the accuracy has been verified by FE simulations. The obtained results in this paper are compared to the relevant theoretical predictions and experimental measurements. It has been demonstrated that the type-I composites have achieved a conductivity that is almost the same as the highest possible theoretical upper limit, and the type-II composites have a conductivity significantly greater than the experimental results of conventional isotropic composite materials.

1. Introduction

Composite materials exist everywhere in our daily lives.^[1] In fact, the bones and many parts of the organs in our body are made of composite materials.^[2,3] Nowadays, super composite materials are becoming more and more highly demanded in many different applications. They are often required to have some highly desired specific properties, e.g., high strength or stiffness, or best possible thermal/electrical conductivity.

The primary objective of this paper is to enhance the isotropic conductivities of two-phase composite materials by structural design. The composite materials are assumed to be made of two homogenous and isotropic materials A and B, with conductivities μ_A and μ_B , and volume fractions f_A and f_B , respectively. For anisotropic composite materials, the largest possible effective conductivity can be easily achieved when the two constituent materials A and B are uniformly arranged in parallel, e.g., sandwich/laminate composites with layers of uniform thickness. This maximum conductivity is obviously in the direction (or plane) parallel to the two materials, and given by the Voigt limit

$$\mu_U = \mu_A f_A + \mu_B f_B \quad (1)$$

where, $f_A + f_B = 1$. The lowest possible conductivity of this type of anisotropic composites is in the direction normal to the plane, and given by the Reuss limit

$$\mu_L = \frac{\mu_A \mu_B}{\mu_A f_B + \mu_B f_A} \quad (2)$$

For isotropic two-phase composite materials, however, the range of the thermal/electrical conductivities is much narrower, and limited by the Hashin and Shtrikman's upper and lower bounds,^[4]

$$\mu_{HS,U} = \mu_A + \frac{f_B}{\frac{1}{\mu_B - \mu_A} + \frac{f_A}{3\mu_A}} \quad (3)$$

$$\mu_{HS,L} = \mu_B + \frac{f_A}{\frac{1}{\mu_A - \mu_B} + \frac{f_B}{3\mu_B}} \quad (4)$$

where it is assumed that $\mu_A \geq \mu_B$.

The Voigt and Reuss limits give the absolute maximum and minimum conductivities, and they are applicable for all different types of materials, including isotropic composites and highly anisotropic composites; while the Hashin and Shtrikman's upper and lower bounds are strictly correct only for isotropic composites.

There are numerous research papers on the conductivities of different types of composites or porous materials containing air or fluid. In this paper, however, the focus is only on isotropic conductivity of two-phase solid composites, and the effects of interfaces and imperfections are not considered. Many people have done theoretical analyses,^[5–18] computational simulations,^[19,20] and experimental measurements^[21–27] on the conductivities of isotropic two-phase materials. The first theoretical prediction for the conductivity of composites

[*] Dr. H. Zhu

School of Engineering, Cardiff University,
Cardiff CF24 3AA, UK
E-mail: zhuh3@cf.ac.uk

Dr. T. Fan, Dr. D. Zhang

State Key Lab of Metal Matrix Composites, Shanghai Jiaotong
University, Shanghai 200240, China

This is an open access article under the terms of the Creative Commons Attribution License, which permits use, distribution and reproduction in any medium, provided the original work is properly cited.

The copyright line of this paper was amended 11 May 2016 after initial online publication.

was given by Maxwell,^[5] which is actually the same as the Hashin and Shtrikman's lower bound (i.e., Eq. 4). Bruggeman^[6] derived an implicit equation for the conductivity of a composite which contains a homogeneous medium and spherical particles in the medium:

$$\frac{\mu_A - \mu_C}{\mu_A - \mu_B} \left(\frac{\mu_B}{\mu_C} \right)^{\frac{1}{3}} = 1 - f_A \quad (5)$$

where μ_C is the effective conductivity of the composite.

Russell^[7] studied the conductivity for high-porosity foams containing a fluid inside the closed cells. Assuming that the pores are cubes of the same size and that the isothermal lines are planes, he obtained the conductivity using a series parallel network:

$$\mu_C = \frac{[f_B^{2/3} \mu_B + (1 - f_B^{2/3}) \mu_A] \mu_A}{(f_B^{2/3} - f_B) \mu_B + (1 + f_B - f_B^{2/3}) \mu_A} \quad (6)$$

where f_B is the pore volume fraction, μ_A and μ_B are the conductivities of the solid and fluid. The predicted results by Equation 6 are actually larger than the Hashin and Shtrikman's upper bound, as can be seen in Figure 5b in the results and discussion part.

Ratcliffe^[8] analyzed approximately 150 sets of data and determined the variation of the individual data points with the correlation, he proposed a prediction for the effective conductivity:

$$\mu_C = \mu_A^{f_A} \mu_B^{1-f_A} \quad (7)$$

Equation 7 is also called the geometric mean model. Fu et al.^[9] theoretically studied the conductivity of open-cell cellular materials using representative unit cell models: a cubic box with a square hole on each of the faces, and a cubic box with a circular hole on each of the faces. Boomsma and Poulikakos^[10] analyzed the conductivity of saturated open-cell metal foams using the idealized body-centered-cubic cell structure. Wang et al.^[11] used a symmetric and interconnected skeleton structural model to predict the thermal conductivity of open-cell foams with hollow and solid struts.

Most theoretical predictions^[6,8-18] for the conductivities of isotropic composites lie between the Hashin and Shtrikman's upper and lower bounds, and are much closer to their lower bound. Giordano^[15] and Duan et al.^[16] have theoretically investigated the effects of particle shape, distribution, and orientation on the conductivities of two-phase composite materials. They^[15,16] obtained the same conductivity as Maxwell's prediction (or the Hashin and Shtrikman's lower bound) for the case when the particles are spherical and randomly distributed; and they also demonstrated that if all the particles are thin and long cylinders (fibers), and are aligned and oriented in the same direction, the composite material exhibits very strong anisotropy

and its conductivity is very close to the Voigt limit in the particle/fiber direction, and close to the Reuss limit in the orthogonal directions.

Bonnecaze and Brady^[19,20] performed numerical simulations on the conductivities of isotropic composites with randomly distributed spherical particles. Weber et al.^[21] experimentally measured the conductivity for composites with randomly oriented particles. Wang et al.^[22] experimentally measured the thermal conductivities of nanoparticle-fluid mixtures. Many other people^[23-27] have also experimentally measured the isotropic conductivities for different types of composites. The simulation results^[19,20] and the experimental results^[21-27] for the conductivities of isotropic materials are much closer to the Hashin and Shtrikman's lower bound than their upper bound. It has been found that the effective conductivities of composite materials can be affected by the locations, orientations, and shapes of their component materials. With favorable structural distribution, the bounds of the effective conductivities of composite materials can be further narrowed.^[15,16,28-30]

In this paper, we will study the isotropic conductivities of two types of specially structured two-phase composite materials. It is demonstrated that the effective conductivity of the type-I composites is approximately the same as the highest possible upper limit for isotropic composites (i.e., the Hashin and Shtrikman's upper limit), and the type-II composites have an effective conductivity significantly greater than the experimentally measured results for isotropic composite materials.

2. Geometrical Structure

2.1. Type-I Composites

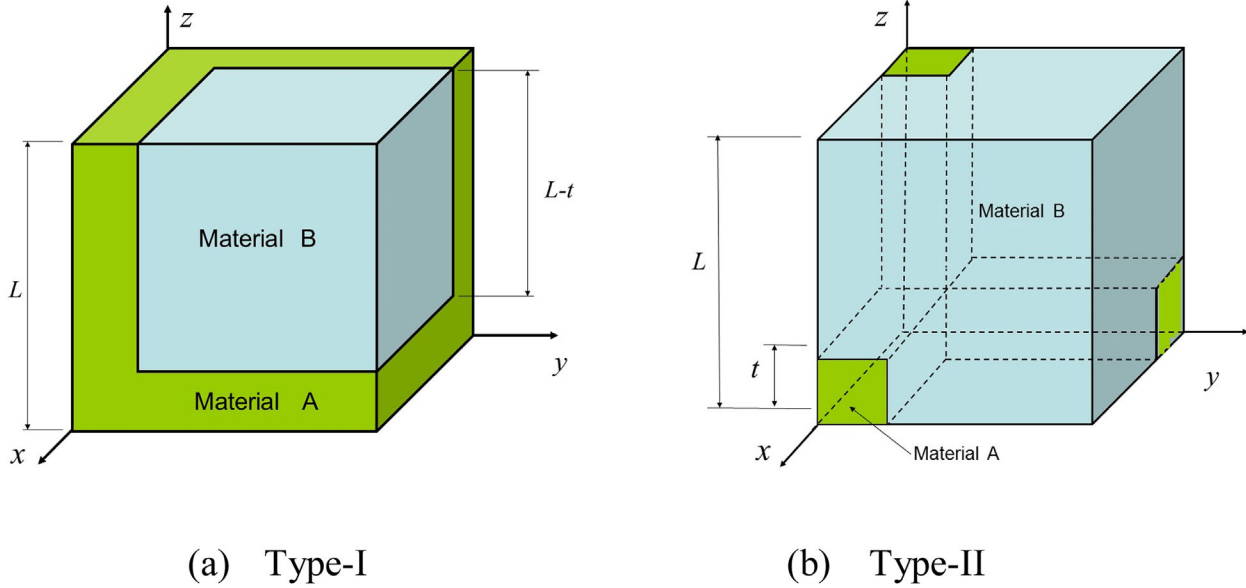
In this type of composites, material A is assumed to have the geometrical structure of a perfectly regular closed-cell foam with a large number of identical cubic cells of edge length L and square cell walls of uniform thickness t ; material B is assumed to be identical cubes of edge length $L - t$, which are located at each of the cell centers of material A. Figure 1a shows a cubic periodic unit representative volume element (RVE) for this type of composites, in which the volume fraction of material A is

$$f_A = 1 - (L - t)^3 / L^3 \quad (8)$$

and the volume fraction of material B is thus $f_B = (L - t)^3 / L^3$. Advanced manufacturing technology, e.g., 3D printing or prototyping,^[31] makes it possible to produce this type of composite materials.

2.2. Type-II Composites

In this type of composites, material A is assumed to have the geometrical structure of a perfectly regular open-cell foam with a large number of identical cubic cells which have uniform edges of length L and square cross-section of side t ; material B is the matrix which fills the space of material A.



(a) Type-I

(b) Type-II

Fig. 1. Cubic periodic representative volume elements (RVEs) of the two types of composite materials.

Figure 1b shows a periodic cubic unit representative volume element (RVE) of this type of composites, in which the volume fraction of material A is

$$f_A = \frac{3t^2}{L^2} - \frac{2t^3}{L^3} \quad (9)$$

and the volume fraction of material B is thus $f_B = 1 - f_A$.

3. Analytical Models

Both types of composites have cubic symmetry^[32,33] and their thermal/electrical conductivities and mechanical properties^[34,35] are obviously the same in the x , y , and z directions. Thus, the conductivities of the two types of composites are isotropic (i.e., the same in all directions). It is very easy and quite straightforward to obtain the analytical results for an overestimated conductivity, μ_2 , and an underestimated conductivity, μ_1 . As the difference between the underestimated and overestimated results is quite small (much smaller than the range of the Hashin and Shtrikman's upper and lower bounds), the mean result, $(\mu_1 + \mu_2)/2$, will thus be taken as our prediction.

3.1. Type-I Composites

To obtain an overestimated conductivity in the z direction, the RVE in Figure 1a is divided into two parts in series. Part (a) is the square wall in the bottom, which is made of only material A and has a side length L and a thickness t . Part (b) is the rest part and composed of two smaller parts in parallel: one is the two connected vertical walls which are made of material A and have a height $L - t$ and a thickness t , and the other is the cubic filler/inclusion which is made of material B and has a side length $L - t$. The overestimated conductivity can thus be obtained as

$$\begin{aligned} \mu_2^I &= \frac{(2L - t)t\mu_A^2 + (L - t)^2\mu_A\mu_B}{\mu_A L(L - t) + \mu_A(2L - t)t^2/L + \mu_B(L - t)^2t/L} \\ &= \frac{(1 - f_B^{2/3})\mu_A + f_B^{2/3}\mu_B}{1 - f_B^{2/3} + f_B + (f_B^{2/3} - f_B)\mu_B/\mu_A} \end{aligned} \quad (10)$$

which is exactly the same as Russell's prediction^[7] given in Equation 6.

To obtain an underestimated conductivity in the z direction, the RVE in Figure 1a is divided into two parts in parallel. Part (a) is the two connected vertical walls which are made of material A and have a height L and a thickness t . Part (b) is the rest part and composed of two smaller parts in series: one is the square wall in the bottom, which is made of material A and has a side length $L - t$ and a thickness t , and the other is the cubic filler/inclusion which is made of material B and has a side length $L - t$. The underestimated conductivity is obtained as

$$\begin{aligned} \mu_1^I &= \frac{(2L - t)t}{L^2}\mu_A + \frac{\mu_A\mu_B}{\mu_A(L - t)/L + \mu_B t/L} \cdot \frac{(L - t)^2}{L^2} \\ &= (1 - f_B^{2/3})\mu_A + \frac{f_B^{2/3}\mu_B}{f_B^{1/3} + (1 - f_B^{1/3})\mu_B/\mu_A} \end{aligned} \quad (11)$$

The predicted thermal/electrical conductivity for the type-I composites is thus obtained as

$$\mu^I = \frac{\mu_1^I + \mu_2^I}{2} \quad (12)$$

3.2. Type-II Composites

To obtain an overestimated conductivity in the z direction, the RVE in Figure 1b is divided into two parts in series. Part (a) is the bottom part of height t and composed of two smaller parts in parallel: one is a parallelepiped which is made of material B and has a height t and a square cross-section of side $L - t$, the other is the connected two horizontal edges which are made of material A and have a total length $2L - t$. The effective conductivity of part (a) in the z direction is $\mu_{(a)}^{\text{II}} = \frac{(2L-t)t}{L^2} \mu_A + \frac{(L-t)^2}{L^2} \mu_B$. Part (b) is the rest part of the RVE in Figure 1b and composed of two smaller parts in parallel: one is the vertical edge which is made of material A and has a length $L - t$ and a square cross-section of side t , the other is the rest which is made of material B. The effective conductivity of part (b) in the z direction is $\mu_{(b)}^{\text{II}} = \frac{t^2}{L^2} \mu_A + (1 - \frac{t^2}{L^2}) \mu_B$. The overestimated conductivity of the type-II composites can be obtained as

$$\mu_2^{\text{II}} = \frac{\mu_{(a)}^{\text{II}} \mu_{(b)}^{\text{II}} L}{(L-t) \mu_{(a)}^{\text{II}} + t \mu_{(b)}^{\text{II}}} \quad (13)$$

To obtain an underestimated conductivity in the z direction, the RVE in Figure 1b is divided into three parts in parallel. Part (a) is the vertical edge which is made of material A and has a length L and a square cross-section of side t . Part (b) is the parallelepiped which is made of material B and has a height L and a square cross-section of side $L - t$. Part (c) is the rest part and composed of two identical parts, each of which is, in turn, composed of two smaller parts in series: one is the horizontal edge which is made of material A and has a length of $L - t$ and a square cross-section of side t , and the other is a vertical square wall which is made of material B and has a side length $L - t$ and a thickness t . The underestimated conductivity of the type-II composites can be obtained as

$$\mu_1^{\text{II}} = \frac{t^2}{L^2} \mu_A + \frac{(L-t)^2}{L^2} \mu_B + \frac{2(L-t)t}{L^2} \frac{\mu_A \mu_B L}{(L-t) \mu_A + t \mu_B} \quad (14)$$

The predicted conductivity for the type-II composites is thus obtained as

$$\mu^{\text{II}} = \frac{\mu_1^{\text{II}} + \mu_2^{\text{II}}}{2} \quad (15)$$

4. Results and Discussion

It makes sense to assume that material A has a larger thermal/electrical conductivity than material B, i.e., $\mu_A/\mu_B \geq 1.0$. For simplicity, the obtained effective conductivity of the composites, μ_C , is normalized by μ_B .

For the type-I composites with fixed volume fractions $f_A = 0.271$ and $f_A = 0.488$, the dimensionless effective conductivities, $\mu_{\text{Present}} = \mu^{\text{I}}/\mu_B$, are obtained from Equation 12 and shown in Figure 2a and b. The Voigt limit (i.e., Eq. 1), Reuss limit (i.e., Eq. 2), and Hashin and Shtrikman's upper and lower bounds are also included for comparison. To validate our predictions from Equation 12, ABAQUS finite element software was used to obtain the effective conductivities for the composites and the dimensionless results μ_{ABAQUS} are also included for comparison. In order to obtain the simulation results for the conductivity of the composites, the cubic periodic RVEs in Figure 1 were partitioned into 8000 DC3D8 elements. All the nodes on the bottom surface were assumed to have the same temperature 120°C , all the nodes on the top surface were assumed to have the same temperature 20°C , and the gradients on all the four side surfaces were assumed to be 0 in their normal directions. This is because the geometrical models in Figure 1a and b can be viewed as one-eighth of the unit cells of the two types of composites (i.e., doubling the dimensions of both L and t in Figure 1a and b does not change the structures and the volume fractions of the two types of composites). Thus, there is no heat flux through each of the four side surfaces due to the symmetry of the structures. The heat flux, W , through the RVEs in the z direction can be directly obtained from ABAQUS simulation, and the effective conductivity of the

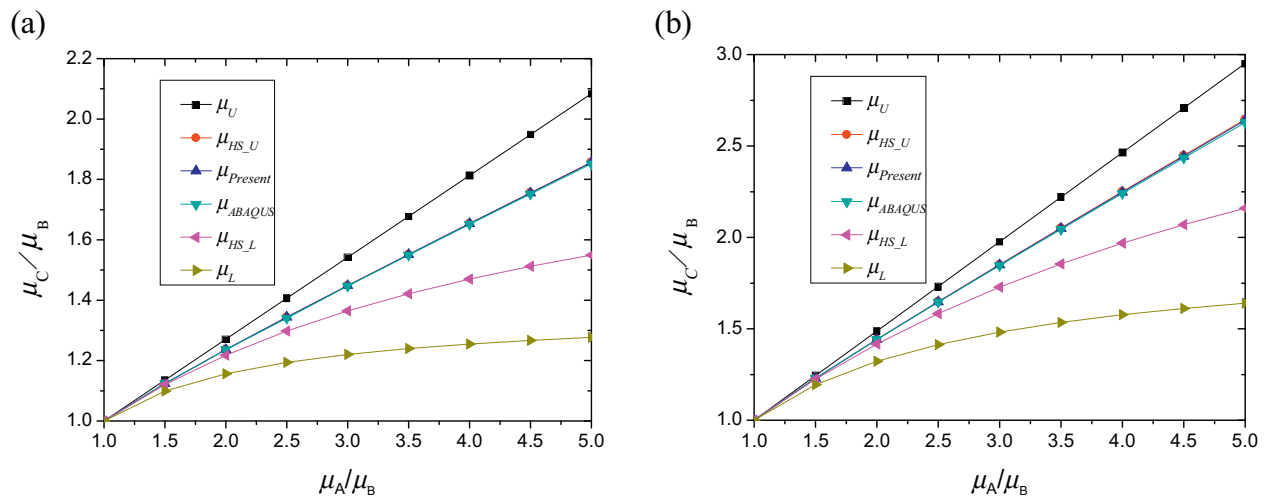


Fig. 2. Effects of μ_A/μ_B on the effective conductivity of type-I composite materials: (a) $f_A = 0.271$; (b) $f_A = 0.488$.

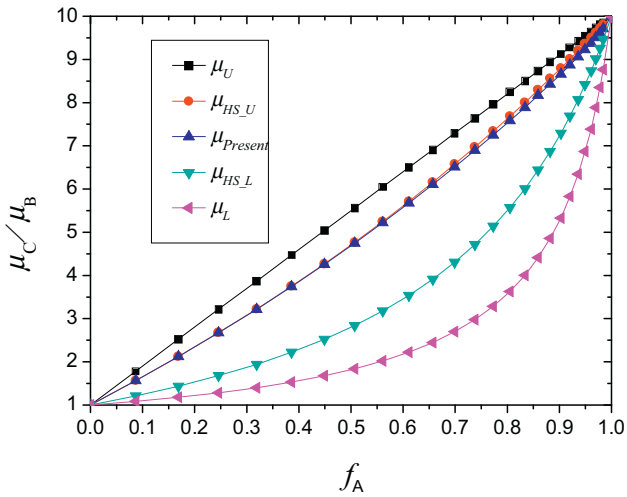


Fig. 3. Effects of f_A on the effective conductivity of type-I composite materials with $\mu_A/\mu_B = 10$.

composites (i.e., RVEs) can thus be obtained as $\mu_C = WL/(\Delta TL^2) = W/(\Delta TL)$, where $\Delta T = 120 - 20 = 100$ °C and L is the side length of the cubic RVEs. As can be seen, our predicted results obtained from Equation 12 are almost the same as the ABAQUS simulation results, indicating that they are very accurate.

Figure 3 shows the relationship between the predicted dimensionless conductivity of the type-I composites and the volume fraction f_A when $\mu_A/\mu_B = 10$, the Voigt limit, Reuss limit, and Hashin and Shtrikman's upper and lower bounds are also included for comparison. Both Figure 2 and 3 demonstrate clearly that the thermal/electrical conductivities of the type-I composites predicted by Equation 12 are almost the same as the Hashin and Shtrikman's upper limit μ_{HS_U} , indicating that the designed geometrical structure shown in Figure 1a has enabled a two-phase composite to achieve the highest possible isotropic thermal/electrical conductivity. It is worthy to note that if $\mu_A/\mu_B < 1.0$, the effective conductivity of the type-I composites is reversed, and very close to lowest

possible limit for isotropic materials (i.e., the Hashin and Shtrikman's lower limit μ_{HS_L}).

For the type-II composites with fixed volume fractions $f_A = 0.104$ and $f_A = 0.50$, the effective dimensionless conductivities, $\mu_{Present} = \mu^{II}/\mu_B$, are obtained from Equation 15 and shown in Figure 4a and b. The Voigt limit (i.e., Eq. 1), Reuss limit (i.e., Eq. 2), Hashin and Shtrikman's upper and lower bounds, and the ABAQUS simulation results μ_{ABAQUS} are all included for comparison. As can be seen, when $f_A = 0.104$, the results obtained from Equation 15 are almost identical to the ABAQUS simulation results, and when $f_A = 0.50$, the predicted results are just very slightly smaller than the ABAQUS simulation results, indicating that Equation 15 can provide very accurate predictions. Figure 5a shows a comparison between our prediction for the conductivity of the type-II composites and the well-known upper and lower bounds. Figure 5b compares our prediction for the conductivity of the type-II composites with the predicted results by some other relevant theoretical models: Russell's model,^[7] Hashin and Shtrikman's upper bound,^[4] Bruggeman's model,^[6] Ratcliffe's model,^[8] and Hashin and Shtrikman's lower bound.^[4] In Figure 5a and b, the effective conductivity is normalized by μ_B and $\mu_A/\mu_B = 10$. As can be seen from Figure 4 and 5, the conductivity of the type-II composite materials is much closer to the Hashin and Shtrikman's upper bound than their lower bound. Russell's model has obviously overestimated the isotropic conductivity because the Hashin and Shtrikman's upper bound^[4] is generally recognized as an unexceedable upper limit for the conductivity of isotropic composites. As the conductivities of the type-I composites are almost identical to the Hashin and Shtrikman's upper bound (see Figure 2 and 3), only the type-II composites are included in Figure 5a and b for comparison. The predicted conductivities from other theoretical models are much lower than our predicted results for the type-II composites, and much closer to the Hashin and Shtrikman's lower bound than to their upper bound.

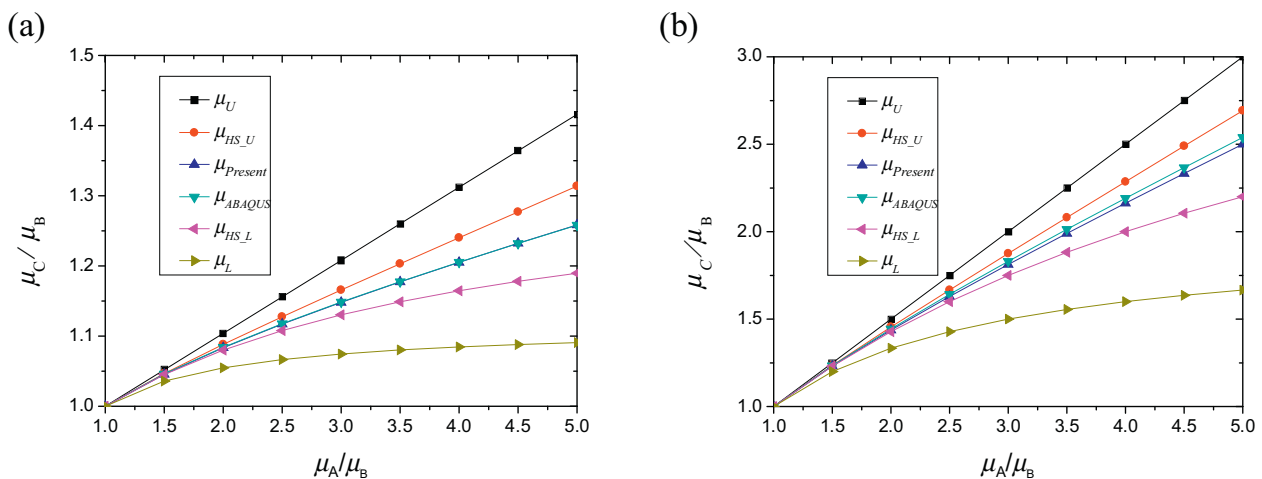


Fig. 4. Effects of μ_A/μ_B on the effective conductivity of type-II composite materials: (a) $f_A = 0.104$; (b) $f_A = 0.5$.

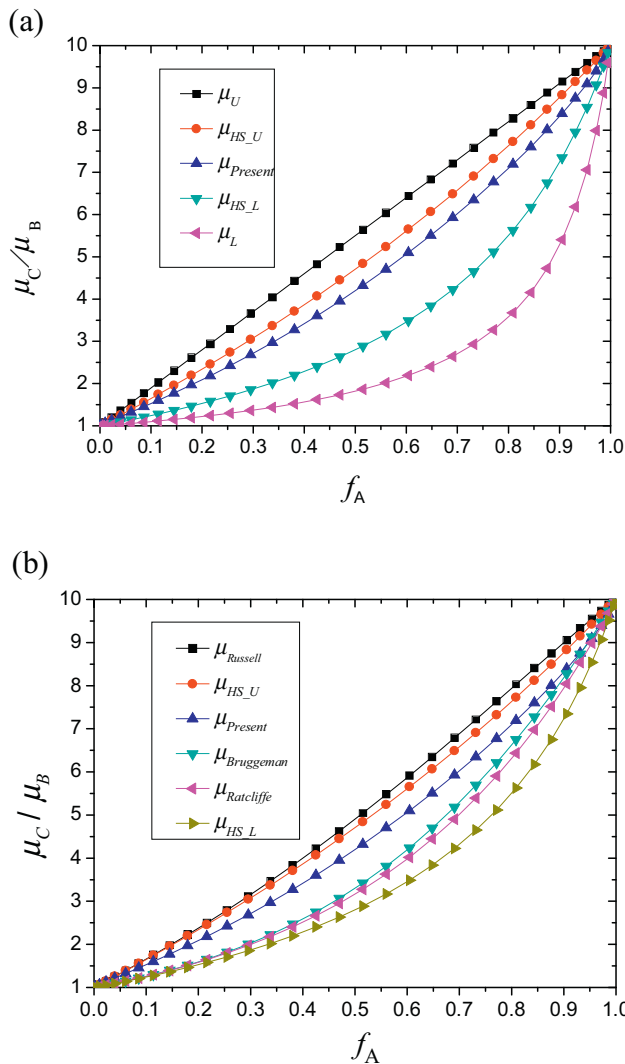


Fig. 5. Effects of f_A on the effective conductivity of type-II composite materials with $\mu_A/\mu_B = 10$. (a) Comparison with classical bounds; (b) comparison with some theoretical models.

Many people^[21–27] have experimentally measured the conductivities of different types of two-phase isotropic composite materials. Frusteri et al.^[23] measured the conductivities of composites with carbon fibers embedded in PCM44, an eutectic mixture of $Mg(NO_3)_2 \cdot 6H_2O$ – $MgCl_2 \cdot 6H_2O$ – NH_4NO_3 , where $\mu_A = 180 \text{ W mK}^{-1}$ and $\mu_B = 0.47 \text{ W mK}^{-1}$. Wong and Bollampally^[24] measured the conductivities of alumina-filled epoxy composites, where $\mu_A = 36 \text{ W mK}^{-1}$ and $\mu_B = 0.195 \text{ W mK}^{-1}$. Mu et al.^[25] measured the conductivities of silicone rubber filled with ZnO particles, where $\mu_A = 60 \text{ W mK}^{-1}$ and $\mu_B = 0.165 \text{ W mK}^{-1}$. Zhang et al.^[26] measured the conductivities of composites with flaky graphite particles of different sizes randomly embedded in polytetrafluoroethylene (PTFE) matrix, where $\mu_A = 135 \text{ W mK}^{-1}$ and $\mu_B = 0.19 \text{ W mK}^{-1}$. Boudenne et al.^[27] measured the conductivities of composites of polypropylene matrix filled with aluminum particles, where $\mu_A = 237 \text{ W mK}^{-1}$ and $\mu_B = 0.239 \text{ W mK}^{-1}$. Figure 6 shows the comparison between our predictions for

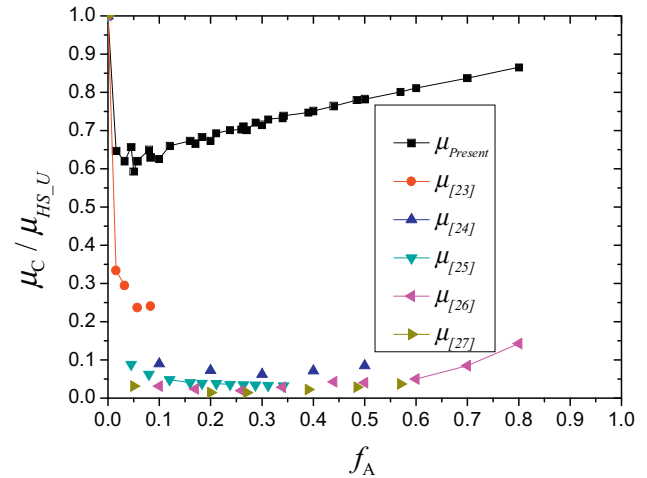


Fig. 6. Comparison between the experimentally measured results^[23–27] and our prediction for the type-II composites. Results are normalized by the Hashin and Shtrikman's upper bound.

the conductivities of the type-II composites and the relevant experimentally measured results for different isotropic composites.^[23–27] As the values of μ_A and μ_B are very different in different experiments,^[23–27] in order to compare those measured results with our predicted results for the conductivities of the type-II composites in a single figure, all the results are normalized by the Hashin and Shtrikman's upper bound (i.e., normalized by Eq. 3). Thus, our predicted relation between the dimensionless conductivity of the type-II composites and f_A is not a smooth curve. This is because for different values of f_A , the values of μ_A and μ_B are different in different experiments. Again, as the conductivities of the type-I composites are almost the same as the Hashin and Shtrikman's upper bound (see Figure 2 and 3), their normalized results would be almost constantly 1.0 and thus not plotted in Figure 6. It can be seen that all the relevant experimentally measured conductivities of isotropic composites are much smaller than the type-II composites, suggesting that the geometrical structure of the type-II composite significantly enhances the isotropic conductivity of two-phase composites.

To the best of our knowledge, all the reported experimental results for the conductivity of conventional isotropic particle or fiber composite materials are always smaller than the results of the type-II composites, and much closer to Hashin and Shtrikman's lower bound. Moreover, the geometrical structures in Figure 1a and b can not only significantly enhance the conductivity of isotropic composites, but also, by combination with the different Poisson's ratios of the two constituent materials, enable the Young's modulus of the composites to be much greater than the Voigt limit.^[34,35] It is noted that other types of composites, e.g., laminate materials, could also have a Young's modulus greater than the Voigt limit because of the effects of the Poisson's ratios.^[36–40] Thus, we could conclude that the type-I structure in Figure 1a can maximize the isotropic conductivity of two-phase composites, and that the type-II structure shown in Figure 1b can

significantly enhance the isotropic conductivity of two-phase composites.

Article first published online: February 29, 2016

Manuscript Revised: February 1, 2016

Manuscript Received: September 24, 2015

-
- [1] D. Hull, T. W. Clyne, *An Introduction to Composite Materials*, Cambridge Press, UK **1996**.
- [2] M. J. Buehler, *Proc. Natl. Acad. Sci.* **2006**, *103*, 12285.
- [3] H. Gao, B. Ji, I. L. Jager, E. Arzt, P. Fratzl, *Proc. Natl. Acad. Sci.* **2003**, *100*, 5597.
- [4] Z. Hashin, S. Shtrikman, *J. Appl. Phys.* **1962**, *33*, 3125.
- [5] J. C. Maxwell, *A Treatise on Electricity and Magnetism*, Clarendon, Oxford **1873**.
- [6] D. Bruggeman, *Ann. Phys.* **1935**, *24*, 636.
- [7] H. W. Russell, *J. Am. Ceram. Soc.* **1935**, *18*, 1.
- [8] E. H. Ratcliffe, *J. Appl. Chem.* **1968**, *18*, 25.
- [9] X. Fu, R. Viskanta, J. P. Gore, *Int. Commun. Heat Mass Transfer* **1998**, *25*, 151.
- [10] K. Boomsma, D. Poulikakos, *Int. J. Heat Mass Transfer* **2001**, *44*, 827.
- [11] J. F. Wang, J. K. Carson, J. Willix, M. F. North, D. J. Cleland, *Acta Mater.* **2008**, *56*, 5138.
- [12] D. J. Jeffrey, *Proc. Roy. Soc. Lond. A* **1973**, *335*, 355.
- [13] G. M. Milton, *Phys. Rev. Lett.* **1981**, *46*, 542.
- [14] H. Hatta, M. Taya, *J. Appl. Phys.* **1985**, *58*, 2478.
- [15] S. Giordano, *J. Electrostat.* **2003**, *58*, 59.
- [16] H. L. Duan, B. L. Karihaloo, J. Wang, X. Yi, *Phys. Rev. B* **2006**, *73*, 174203.
- [17] H. L. Duan, B. L. Karihaloo, *Phys. Rev. B* **2007**, *75*, 064206.
- [18] E. W. Tiedje, P. Guo, *J. Mater. Sci.* **2014**, *49*, 5586.
- [19] R. T. Bonnecaze, J. F. Brady, *Proc. Roy. Soc. Lond. A* **1990**, *430*, 285.
- [20] R. T. Bonnecaze, J. F. Brady, *Proc. Roy. Soc. Lond. A* **1991**, *432*, 445.
- [21] L. Weber, J. Dorn, A. Mortensen, *Acta Mater.* **2003**, *51*, 3199.
- [22] X. Wang, X. Xu, S. U. S. Choi, *J. Thermophys. Heat Transfer* **1999**, *13*, 474.
- [23] F. Frusteri, V. Leonardi, S. Vasta, G. Restruccia, *Appl. Therm. Eng.* **2005**, *25*, 1623.
- [24] C. P. Wong, R. S. Bollampally, *J. Appl. Polym. Sci.* **1999**, *74*, 3396.
- [25] Q. H. Mu, S. Y. Feng, G. Z. Diao, *Polym. Compos.* **2007**, *28*, 125.
- [26] G. Zhang, Y. Xia, H. Wang, Y. Tao, G. Tao, S. Tu, H. Wu, *J. Compos. Mater.* **2010**, *44*, 963.
- [27] A. Boudenne, L. Ibos, M. Fois, E. Gehin, J. C. Majeste, *J. Polym. Sci. Part B* **2004**, *42*, 722.
- [28] C. P. Ponte, *Phys. Rev. B* **2001**, *64*, 214205.
- [29] S. Torquato, *Random Heterogeneous Materials; Microstructure and Macroscopic Properties*, Springer-Verlag, New York **2012**.
- [30] J. R. Willis, *J. Mech. Phys. Solids* **1977**, *25*, 185.
- [31] S. Derby, *Science* **2012**, *338*, 921.
- [32] C. N. Reid, *Deformation Geometry for Materials Scientists*, Pergamon, Oxford **1972**.
- [33] H. X. Zhu, J. F. Knott, N. J. Mills, *J. Mech. Phys. Solids* **1997**, *45*, 319.
- [34] H. X. Zhu, T. X. Fan, D. Zhang, *Sci. Rep.* **2015**, *5*, 14103.
- [35] H. X. Zhu, T. X. Fan, C. H. Xu, D. Zhang, submitted for publication, **2016**.
- [36] R. S. Lakes, *Science* **1987**, *235*, 1038.
- [37] G. W. Milton, *J. Mech. Phys. Solids* **1992**, *40*, 1105.
- [38] B. Liu, X. Feng, S. M. Zhang, *Compos. Sci. Tech.* **2009**, *69*, 2198.
- [39] J. N. Grima, R. Cauchi, R. Gatt, D. Attard, *Compos. Struct.* **2013**, *106*, 150.
- [40] T. Streck, H. Jopek, M. Nienartowicz, *Phys. Status Solidi B* **2015**, *252*, 1540.
-